Energy & Environmental Science

RSC Publishing

PAPER

View Article Online
View Journal | View Issue

Cite this: *Energy Environ. Sci.*, 2013, **6**, 1573

Achieving high efficiency and cyclability in inexpensive soluble lead flow batteries†

Michael G. Verde,[a] Kyler J. Carroll,[a] Ziying Wang,[a] Aaron Sathrum[b] and Ying Shirley Meng*[a]

Received 25th February 2013
Accepted 13th March 2013

DOI: 10.1039/c3ee40631h

www.rsc.org/ees

Here we report on the significant improvements made in the energy efficiency and cycle life of full-cell soluble lead flow batteries (SLFBs). We describe energy efficiency loss mechanisms, particularly in context to the deposition of PbO_2 at the positive electrode. The morphology and crystal structure of deposits formed at the positive electrode, under galvanostatic and potentiostatic conditions, were characterized using both powder X-ray diffraction (XRD) and scanning electron microscopy (SEM). Rietveld refinements were performed to quantitatively determine the phase fraction of α- and β-PbO_2 formed. In addition, electrochemical impedance spectroscopy (EIS) was used to describe the charge-transfer reaction occurring at the positive electrode during conditions that promote the formation of various PbO_2 morphologies. These features were used to evaluate and predict the long-term cycling stability of SLFBs as well as to diagnose potential problems arising during battery operation. We demonstrate that conditions optimized to preferentially deposit nanoscale PbO_2 leads to long battery lifetimes, exceeding 2000 cycles at 79% energetic efficiency.

Broader context

Motivated by booms in the electronics industry and the increased demand of hybrid and electric vehicles, the development of high energy density storage systems has been hotly pursued in recent years. In addition, the economic and geopolitical instability of oil has also accelerated the demand for large-scale energy storage systems for use in smart grids, to assist in load leveling, peak shaving and frequency regulation for renewable energy systems such as solar and wind. For these applications, however, high energy density is not necessarily the most determining feature for an energy storage system to possess. Considerations such as cost, durability, longevity and flexibility in design and operation take precedence since their size and weight in large-scale applications are not restricted. For these reasons, flow batteries have begun to garner a great deal of attention. Perhaps the most simple and inexpensive of these is the soluble lead flow battery (SLFB). Here we describe critical conditions necessary to achieve extended lifetimes, greater than 2000 cycles, in these batteries.

Introduction

A particularly attractive flow battery system for large-scale applications is the soluble lead flow battery (SLFB). This is mainly due to the simplicity in its design, leading to quite inexpensive architectures. In typical flow batteries, the electroactive species are dissolved in an electrolyte, as opposed to existing in the electrodes themselves. Due to the incompatible redox chemistry occurring at each electrode, however, most flow batteries require two distinct electrolyte solutions, the catholyte and anolyte, being isolated from one another by a separator.[1] These ion-selective separators are not only costly, but are often responsible for eventual flow battery failure, as they are susceptible to cross-contamination.[2] The SLFB provides a considerable advantage, therefore, by not requiring one.

A general schematic of a SLFB is shown in Fig. 1. It shows a single electrolyte solution, typically composed of lead methanesulfonate and methanesulfonic acid, being pumped from a reservoir and through housing possessing the electrodes. This modular design, separating the electroactive material from the electrodes and thereby separating energy and power components, respectively, is an advantage of flow batteries in general, making them highly flexible. The fact that SLFBs possess only one electrolyte is significantly more advantageous, however, because in addition to eliminating the need for an ion-selective membrane, it eliminates the need for a second pump and all other housing and electronics that a second electrolyte would require. The balance of the plant for a SLFB is, therefore, considerably cheaper than other flow battery designs, which are already less expensive than alternatives such as lithium-ion.[3]

The reason SLFBs are uniquely apt to operate using a single electrolyte is because a single species, lead(II) ion (Pb^{2+}), is both oxidized and reduced upon charging the battery. The half-cell and full-cell reactions are:

Negative electrode reaction – ($E^0 = -0.13$ V/SHE)

[a]*Department of NanoEngineering, University of California San Diego, La Jolla, CA 92093, USA. E-mail: mverde@ucsd.edu; shmeng@ucsd.edu*

[b]*General Atomics, San Diego, CA 92121, USA*

† Electronic supplementary information (ESI) available: See DOI: 10.1039/c3ee40631h

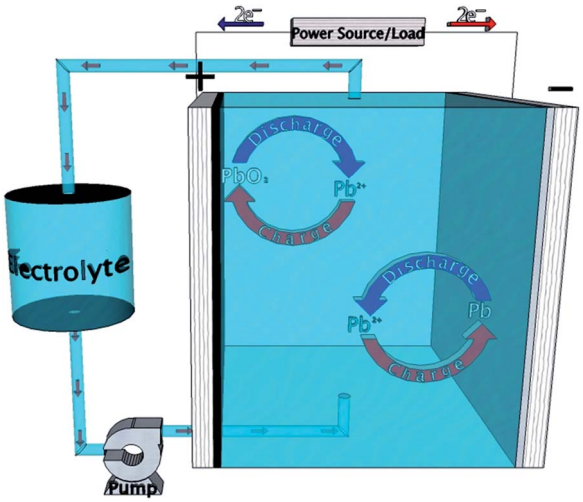

Fig. 1 General schematic of a soluble lead flow battery (SLFB), consisting of an electrolyte reservoir, pump, and electrode housing.

$$Pb^{2+} + 2e^- \underset{\text{discharge}}{\overset{\text{charge}}{\rightleftharpoons}} Pb \quad (1)$$

Positive electrode reaction – ($E^0 = 1.46$ V/SHE)

$$Pb^{2+} + 2H_2O \underset{\text{discharge}}{\overset{\text{charge}}{\rightleftharpoons}} PbO_2 + 4H^+ + 2e^- \quad (2)$$

Full-cell reaction – ($E^0 = 1.59$ V/SHE)

$$2Pb^{2+} + 2H_2O \underset{\text{discharge}}{\overset{\text{charge}}{\rightleftharpoons}} PbO_2 + Pb + 4H^+ \quad (3)$$

Upon charge, Pb^{2+} dissolved in solution is oxidized into solid lead(IV) oxide (PbO_2) at the positive electrode and reduced to metallic lead (Pb) at the negative electrode. Upon discharge, PbO_2 and Pb undergo the reverse redox reaction to dissociate back into Pb^{2+}. This reaction chemistry is distinct from the traditional lead-acid battery, which proceeds *via* a solid–solid redox reaction between lead(II) sulfate ($PbSO_4$) and PbO_2/Pb, at the positive and negative electrodes, respectively.[4] The use of methanesulfonic acid is to both prevent the formation of $PbSO_4$, which can be problematic, and provide a "greener" alternative to sulfuric acid based electrolytes.[5]

In a series of recent papers, Pletcher *et al.* established much of the work leading to SLFBs as they exist today.[6–14] Those studies provide a very thorough analysis of Pb and PbO_2 deposition under an array of conditions, such as electrolyte composition, electrode substrate, temperature, and current density. While optimized full-cells operating at a current density of 10 mA cm^{-2} could achieve 100–200 cycles, lifetimes dropped below 100 cycles at 20 mA cm^{-2} with energetic efficiencies between 60 and 65%.[13,15] Those are relatively poor statistics compared to other flow battery technologies, such as vanadium redox battery, however, which are able to boast energetic efficiencies of 80% for over 1000 cycles.[16] It has been determined that the two major problems associated with SLFBs are dendrite growth of Pb at the negative electrode and the partial irreversibility of PbO_2 at the positive electrode.[7] The use of leveling agents such as sodium lignosulfonate and hexadecyltrimethylammonium cation ($C_{16}H_{33}(CH_3)_3N^+$) has been shown to mitigate Pb dendrite formation,[8,10] but overcoming inefficiency at the positive electrode continues to be a problem.

Optimization of the Pb^{2+}/PbO_2 couple at the positive electrode has been a more challenging task than that of the Pb^{2+}/Pb couple at the negative electrode because of the complexity of reactions occurring at the former. This is reflected in the overpotential of each half-reaction — being only ~90 mV at the negative electrode, but ~450 mV at the positive electrode.[6] The considerably higher overpotential resulting at the positive electrode has been explained in terms of a high concentration polarization by reaction intermediates formed there.[17] In addition to voltaic inefficiency, current inefficiencies partially prevail due to a competing oxygen evolution reaction (OER), at even moderately high current densities, typically greater than 50 mA cm^{-2}, depending upon the electrolyte composition.[11] Several possible mechanisms have been put forth as to the nature of the OER in this system,[17,18] but the most general form is:

($E^0 = 1.23$ V/SHE)

$$2H_2O \rightarrow O_2 + 4H^+ + 4e^- \quad (4)$$

This undesirable side reaction can be minimized by low current density charging, but a considerable degree of current efficiency is still lost because of the incomplete reduction of PbO_2, upon discharge.[6] In many cases, nearly all the lost current efficiency can be accounted for by the PbO_2 mass left behind on the positive electrode after discharge.[13]

The critical nature of this incomplete reduction and the factors contributing to it are the focus of this paper. Previous studies have discussed the likely formation of oxygen deficient PbO_x species, upon discharge.[19] The exact stoichiometry of such species are unclear, however, as only qualitative studies suggest $1 \leq x \leq 2$.[9] Oxygen deficiency in PbO_2 is prevalent[20] and the formation of such species is likely, as models incorporating them accurately predict the unique voltage profile of SLFBs.[21] In addition to the formation of PbO_x, two distinct polymorphs of PbO_2 are known to form at the positive electrode; they are the orthorhombic α-PbO_2 and tetragonal β-PbO_2. Using XRD, Walsh *et al.* have described the preferential formation of one polymorph over the other, under a variety of conditions.[12,22] They concluded that pure α-PbO_2 forms during initial SLFB cycling, but a mixture of each polymorph forms upon later cycles, leading to battery failure. We offer an alternative hypothesis, however, by performing Rietveld refinement on PbO_2 XRD data and considering effects such as preferred crystallite orientation, size, and strain. We propose that efficient and long cycle life is not dependent upon the formation of α-PbO_2, as has been suggested, but relies much more heavily on the morphology of PbO_2 formed. We show that both polymorphs are present upon initial cycling and that their nanoscale morphology is a more critical and determining feature for battery success. We carefully analyze the relationship between long-term performance and battery charging potential, specifically highlighting the relationship between that potential and the morphology of

PbO_2 formed. In optimizing conditions to preferentially form nanoscale PbO_2 we show that SLFBs can achieve more than 2000 cycles at 79% energetic efficiency.

Experimental

Materials and reagents

Electrolytes used in all electrochemical cells were prepared using water from a Millipore ICW-3000 system (18 MΩ cm resistivity), reagent grade lead methanesulfonate ($Pb(CH_3SO_3)_2$), Aldrich 50 wt% in H_2O, and ≥99.5% methanesulfonic acid (CH_3SO_3H), Sigma-Aldrich. Electrolyte compositions always consisted of 0.7 M $Pb(CH_3SO_3)_2$ and 1.0 M CH_3SO_3H, which was chosen to optimize Pb^{2+} solubility and pH during the 1 h charge–discharge windows that batteries were subject to. The solubility and, therefore, energy density of SLFBs are intimately related to the electrolyte pH,[6] which can fluctuate considerably during cycling; according to reaction (3) it is shown that the concentration of H^+ in solution increases twice as fast as the oxidation and reduction of Pb^{2+} into PbO_2 and Pb, respectively.

Electrochemical testing

All full-cell SLFBs were assembled and electrochemically tested by submerging graphite electrodes, spread ¼″ apart, in stirred cylindrical vessels filled with 140 mL of electrolytes; each electrode had an exposed surface area of 2.5 cm × 3.5 cm. Both galvanostatic and potentiostatic cycling tests were performed using an Arbin BT2000 battery testing system. Electrodes were consistently subject to a current density of 20 mA cm^{-2} and discharged to 1.1 V. The electrochemical performances of batteries were evaluated by three main criteria: (1) Coulombic efficiency (η_C), the ratio of the average discharge capacity ($Q_{discharge}$) to the average charge capacity (Q_{charge}); (2) voltaic efficiency (η_V), the ratio of the average discharge voltage ($V_{discharge}$) to the average charge voltage (V_{charge}); (3) energetic efficiency (η_e), the average discharge energy ($E_{discharge}$) to the average charge energy (E_{charge}).

$$\eta_C = \frac{Q_{discharge}}{Q_{charge}} \quad (5)$$

$$\eta_V = \frac{V_{discharge}}{V_{charge}} \quad (6)$$

$$\eta_e = \frac{E_{discharge}}{E_{charge}} \quad (7)$$

Scanning electron microscopy

Following electrochemical cycling and prior to other forms of characterization, deposited anode and cathode materials were rinsed with deionized H_2O while still adhered to each electrode. Deposits were dried in a vacuum at room temperature. Scanning electron microscopy (SEM) was performed on the material still adhered to electrodes, with no further treatment besides washing with water. Images were collected using a Phillips XL30 ESEM at an accelerating voltage of 20 kV.

X-ray diffraction

X-ray diffraction (XRD) measurements were performed using a Bruker D8 advance diffractometer with a Bragg–Brentano θ–2θ geometry and a Cu Kα source ($\lambda = 1.54$ Å). Samples were scanned from 10° to 80° with a scan rate of 0.025° per second. XRD was performed on deposits that had been scraped off of the electrode and ground to a fine powder. A reflection peak for graphite, space group $R\bar{3}m$ R, is present in all XRD spectra, as it was not possible to completely exclude graphite from scraped off PbO_2 deposits. Removing and grinding PbO_2 was necessary in order to quantitatively determine the relative abundance of various PbO_2 phases deposited on the positive electrode; otherwise, due to texturing of as-deposited PbO_2, preferred growth orientations of specific crystal planes skew XRD peak intensities.[12,23] Rietveld refinement was performed using GSAS/EXPGUI software.[24]

Electrochemical impedance spectroscopy

Electrochemical impedance spectroscopy (EIS) was performed using a Solartron 1287 system coupled with a Solartron 1260 frequency response analyzer. The full-cell SLFBs described above were analyzed using EIS, in conjunction with a third, Ag/AgCl, reference electrode. Graphite was, therefore, used as both working and counter electrodes. The impedance of the positive electrode was measured at various fixed potentials, using AC amplitude of 10 mV. Fixed potentials of 1.44, 1.54, and 1.64 V *vs.* Ag/AgCl were applied during EIS measurements, without allowing the cell to equilibrate at OCV. Spectra were obtained in the frequency range of 10^{-2} Hz to 10^5 Hz. Equivalent circuit modeling was performed using the ZView impedance software package.

Results and discussion

Electrochemical indications of failure

A common deterioration mechanism of SLFBs is represented by their electrochemical efficiencies (Fig. 2a). The critical feature in the plot of Fig. 2a, highlighted in green, occurs when the battery nears 90 cycles. At that point there is simultaneous rise in voltaic efficiency and decline of Coulombic efficiency. The rapid drop in Coulombic efficiency is not offset by the small increase in voltaic efficiency, therefore resulting in an overall decrease in energetic efficiency. This marked "inflection", or simultaneous increase in voltaic efficiency and decrease in Coulombic efficiency, is a unique characteristic of SLFBs. It indicates a dramatic decrease in cell performance and accelerated failure.

To more thoroughly describe the electrochemical characteristics of the battery during this sudden change in efficiency, we highlight three points within the green box and inset of Fig. 2a: (1) before the inflection, at the 80th cycle; (2) during the inflection, at the 90th cycle and (3) after the inflection, at the 95th cycle. The charge–discharge voltage of each of these cycles is plotted in Fig. 2b. This figure shows that before the efficiency inflection, the charge voltage profile consists of a major plateau at ~2.0 V. Preceding that plateau, but during the same cycle,

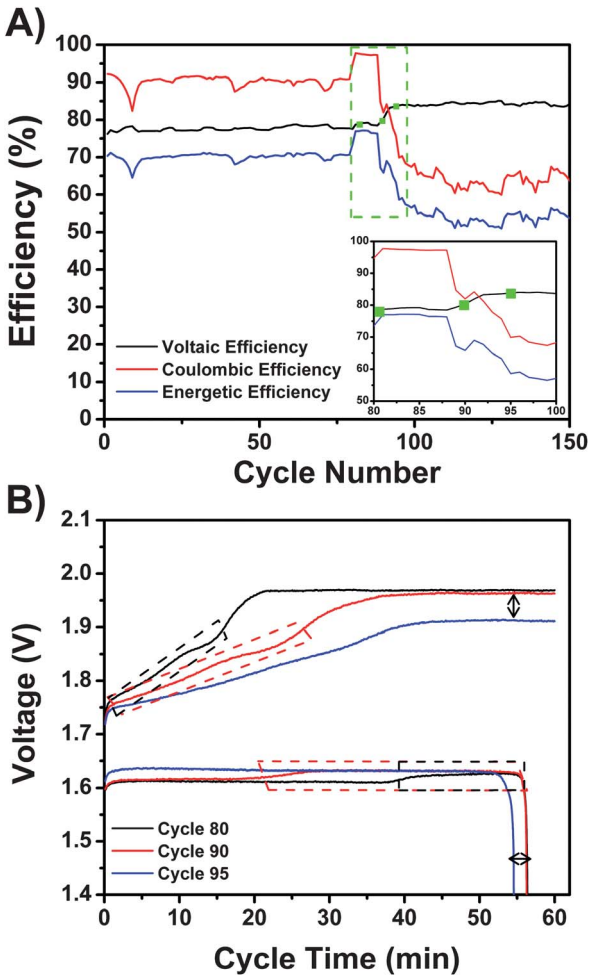

Fig. 2 (A) Electrochemical efficiencies of SLFB. The dotted region highlights the inset, which focuses on 3 specific cycles. (B) Charge–discharge profiles of the 3 cycles indicated by the inset above.

there exists a sloping region beginning at ~1.75 V and a smaller plateau ~100 mV higher. The shape of the voltage profile at the 80th cycle is fairly representative of previous cycles. Upon approaching the efficiency inflection, however, the higher voltage plateau becomes shorter and the sloping region becomes longer, as seen in the 90th charge voltage profile. After the inflection, the high voltage plateau is no longer met. A major voltage plateau still occurs in the 95th cycle, but it has reduced by ~75 mV, as indicated by the vertical arrow in Fig. 2b.

The horizontal arrow in Fig. 2b indicates that the discharge time of the 95th cycle has decreased. Before the efficiency inflection, the duration of discharge is relatively constant. After the inflection, however, it is consistently lower. The charge time and therefore, the amount of Pb and PbO_2 being deposited on each electrode remain constant in all cycles. The decrease in both discharge time and Coulombic efficiency suggests that an increasing amount of unreacted deposit remains on the electrodes after each cycle. The accelerated accumulation of these deposits can be physically observed after the efficiency inflection. The major feature associated with this capacity loss is the depression of the high voltage plateau. Extension of the sloping region during charge cycling results in slightly lower discharge overpotentials, as shown by the black and red dotted regions in Fig. 2b. Only when the original position of the high voltage plateau fails to be met, however, does the capacity begin to considerably fade. We hypothesize that the major problem associated with the depression or elimination of the original voltage plateau is a change in PbO_2 morphology, which is not conducive to efficient dissolution.

We specify formation of PbO_2 at the positive electrode because the shape of the full-cell voltage is a reflection of the Pb^{2+}/PbO_2 half-cell potential. The distinct low and high voltage charging regimes are exclusively present in Pb^{2+}/PbO_2 half-cell measurements.[6] In addition, the low voltage regime arises only after PbO_2 reduction. Several groups have suggested that the reduction of PbO_2 into Pb^{2+}, as described in reaction (2), is not complete.[19,22] It has been proposed that PbO_2 is partially reduced to an oxygen deficient form of PbO_2 (PbO_x, $1 \leq x \leq 2$). The low sloping portion of subsequent charge voltages may, therefore, be due to more easily oxidized PbO_x species into PbO_2. The mechanism and characterization of incomplete PbO_2 reduction has been qualitatively explored using electrochemical[25] and energy dispersive X-ray spectroscopy (EDS)[9] measurements, but quantitative analysis has yet to be performed. An alternative hypothesis proposed by Oury *et al.* suggests that the low voltage regime is instead due to a change in electrode surface area.[26] They suggest that the morphology of PbO_2 left behind upon discharge increases surface area and effectively decreases the current density and resulting overpotential. In either case, further characterization of the material deposited at low voltage would be invaluable, since extension of the low charging voltage or any other mechanism resulting in depression of the initial plateau leads to very poor energetic efficiency.

Characterization of potentiostatically charged cells

In order to more directly elucidate the morphological and phase characteristics associated with the different voltage regimes, batteries were potentiostatically charged at 1.8, 1.9, and 2.0 V. Fig. 3 shows the electrochemical characteristics of three batteries charged at these fixed potentials, for 1 h. This figure shows both the charging voltage and the corresponding potentiostatic current–time transients. Following the initial double-layer charging current, the current of the battery charged at 1.9 V increases exponentially, suggesting progressive nucleation.[29] The current of the battery charged at 2.0 V increases very rapidly and linearly, however, suggesting instantaneous nucleation. Comparing the time required to reach maximum current, it is shown how long it takes nuclei to fully overlap one another and completely cover the electrode surface.[30] This occurs at ~2 minutes into charging at 2.0 V, ~9 minutes after charging at 1.9 V, and never happens during the 1 hour charging period at 1.8 V. These results suggest that at 2.0 V, a large number of nuclei quickly form and coalesce to create layers of nanoparticles. At lower voltages, however, fewer nuclei form and grow, as new nuclei continue to form on the electrode surface. This follows a first order approximation of the nucleation law for a uniform probability with time.[30]

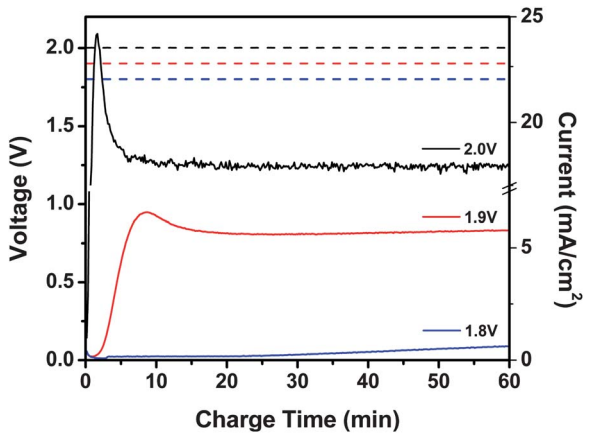

Fig. 3 Voltage (dotted lines) and current–time transients (solid lines) of three SLFBs, potentiostatically charged at 1.8 V (blue), 1.9 V (red), and 2.0 V (black), for 1 h.

Interpretations of the potentiostatic current–time transients are supported by positive electrode SEM images shown in Fig. 4 and 6. The latter represents particle morphologies of PbO_2 deposited after the 1 h potentiostatic charge conditions. They show that at 1.8 V charging, growth is favored, as large *pyramidal* PbO_2 structures were formed. In addition, nuclei have not completely overlapped, as the graphite substrate is still visible. Particle sizes decreased at 1.9 V charging, however, and resulted in a more *cubic* morphology. This specific trend in the shape and morphology of electrodeposited materials, as a function of applied overpotential, has been demonstrated in similar electrolyte and crystal systems.[31] At 2.0 V charging, a uniform, nanoscale morphology, consisting of ellipsoid nanoparticles or "nanorice",[27] was formed. These results are consistent with galvanostatically charged batteries, as shown in Fig. S1 and S2.† Those figures show that when a charging potential of 2.0 V is met, nanoscale PbO_2 is consistently formed. Even upon cycling, when larger PbO_2 particles are initially formed at lower voltages, nanoscale PbO_2 is immediately formed on top when 2.0 V charging resumes.

Fig. 4 shows that trends in particle shape and morphology at each voltage are maintained over extended charge periods as well. Longer charge times were necessary at low voltages to deposit an appreciable amount of PbO_2 for XRD analysis. Whereas a capacity of 1.37×10^{-1} A h is achieved after a 1 h charge at 2.0 V, only 2.3×10^{-3} A h is met after 1 h charge at 1.8 V. The potentiostatic current–time transients of cells subject to an extended charge for XRD analysis are shown in Fig. S3.† The XRD of PbO_2 deposited at each potential is shown in Fig. 5. Vertical dotted lines indicate reflections of pure α- and β-PbO_2 according to the International Crystal Structure Database (ICSD). These two polymorphs are very similar to one another, as both are comprised of Pb^{4+} within distorted octahedra, possess similar Pb–O bond lengths, and differ in standard reduction potential by less than 10 mV.[28]

Fig. 5 shows that upon a single charge at 1.8, 1.9, or 2.0 V, a mixture of α- and β-PbO_2 is always formed. Several groups have reported qualitative analyses suggesting that β-PbO_2 preferentially forms at low charging current densities.[12,22] We performed Rietveld refinement to quantitatively determine that the ratio of α- to β-PbO_2 deposited at 1.8 V is 41 : 59, respectively. At the comparatively higher current density applied during 1.9 V charging, the ratio of α- to β-PbO_2 was determined to be 97 : 3, respectively. Rietveld refined phase fractions, as well as fitted lattice parameters and reliability factors, are shown in Table 1. It is generally rare, however, to form such a high percentage of α-PbO_2 in acidic solutions.[32,33] Despite this, the literature commonly suggests that α-PbO_2 forms in equal and to often-greater degrees than β-PbO_2 in the acidic electrolyte of SLFBs.[22]

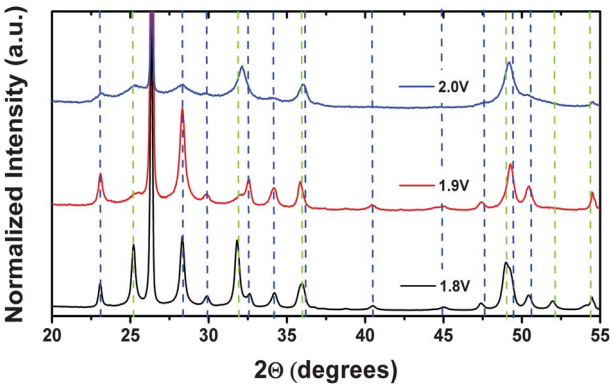

Fig. 5 XRD patterns of positive electrode deposits from SLFBs, potentiostatically charged at 1.8 V (black), 1.9 V (red), and 2.0 V (blue), for 1 h. Dotted lines represent standard XRD reflections of α-PbO_2 (blue) and β-PbO_2 (green). The peak at 26° corresponds to the graphite substrate.

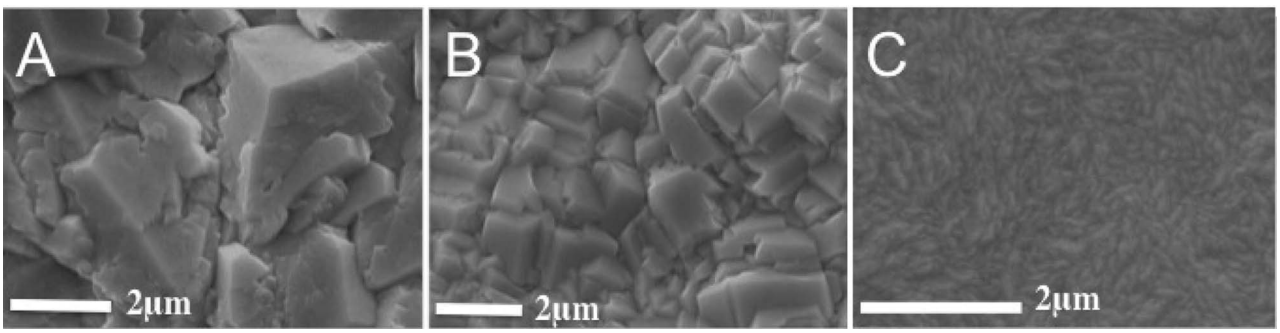

Fig. 4 SEM images of positive electrode deposits from SLFBs potentiostatically charged at (A) 1.8 V, (B) 1.9 V, and (C) 2.0 V.

At 2.0 V charging, however, it is clear that XRD peaks have become significantly broadened. Considering the very small particle sizes formed at 2.0 V (Fig. 4), it is not surprising that decreased crystallite dimension and/or strain exist. Using FWHM parameters, an estimation of crystallite sizes, based on the Scherrer equation, was determined to be 9 nm. Due to the slightly lower reduction potential of β-PbO_2, it is possible that it forms smaller nuclei and crystallite sizes before α-PbO_2. A decrease in β-PbO_2 peak intensity does not necessarily imply, therefore, that less β-PbO_2 exists, it could mean that β-PbO_2 crystallite sizes have simply decreased, relative to α-PbO_2. Indeed when the XRD peaks of α-PbO_2 have broadened during 2.0 V charging, the relative peak intensities are much more proportional to β-PbO_2. The largest reflections, at ~32.0, 36.5, and 49.0° result from the overlap of α- and β-PbO_2 peaks. Fig. S4a and b† show that β-PbO_2 is clearly present during the initial cycles of galvanostatically charged cells as well. These results suggest that maintaining the initial voltage plateau at ~2.0 V is critical to ensure the deposition of nanoscale PbO_2, at the same time it is important to point out that α-PbO_2 is not exclusively present.

Electrochemical impedance spectroscopy

To further describe and gain insight into the electrochemical deposition of PbO_2, as it relates to the applied overpotential, we performed electrochemical impedance spectroscopy (EIS) on full-cells. Using the positive electrode as the working electrode, impedance was measured at 1.44, 1.54, and 1.64 V *vs.* Ag/AgCl. These voltages were chosen as they correspond to the full-cell potentials described previously – 1.8, 1.9, and 2.0 V. Fig. 6a represents the Nyquist plots obtained from those measurements, which were fit to a base equivalent circuit model, shown in the inset. The equivalent circuit used in fitting contains a resistor (R_1 – solution resistance) followed by an RC circuit in parallel. The RC circuit corresponds to a resistor (R_2 – charge-transfer resistance) and a constant phase element (CPE), which was used in place of an ideal capacitor to incorporate changes in the electrode such as surface area. Other groups have reported the use of a second RC circuit to incorporate effects of the OER occurring at the positive electrode.[18] We did not, however, because evidence suggests the OER is a minor side-reaction occurring in our solution composition and with the relatively low current densities applied in our study.[11]

Fig. 6a shows that at each voltage applied, a single semicircle ensues, indicating a single charge-transfer event. As the voltage is increased, the semicircle becomes shorter and more depressed. Electron transfer due to the Pb^{2+}/PbO_2 half-reaction

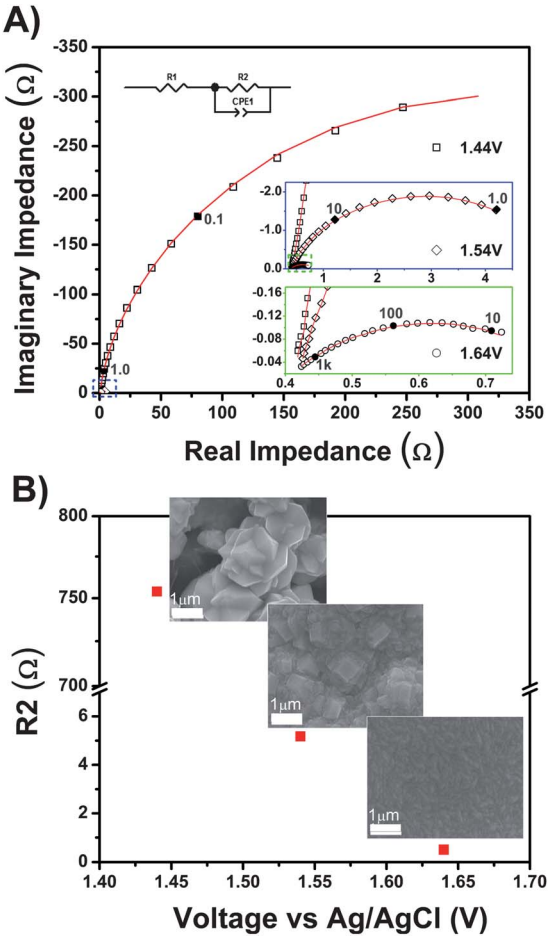

Fig. 6 (A) Nyquist plots from EIS measurements of SLFBs charged at 1.44 V, 1.54 V (blue inset), and 1.64 V (green inset) *vs.* Ag/AgCl reference electrode. Selected AC frequencies are indicated by shaded points. The red line indicates equivalent circuit fit using the model shown by the inset. (B) Charge-transfer resistance (R_2) from fits and associated SEM images of PbO_2 formed at those voltages.

proceeds faster, as the semicircles develop at higher frequencies; at similar positions along the semicircles formed by each 100 mV increase in overpotential, the AC frequencies highlighted are shown to increase by more than an order of magnitude. The enhanced reaction kinetics is quantitatively shown in Fig. 6b, which represents the charge-transfer resistance at each voltage.

The charge-transfer resistance (R_2) is shown to drop off rapidly with increasing overpotential, at a rate described by the Butler–Volmer equation.[34] The SEM images shown in Fig. 6b lend support to the interpretation of nucleation and growth

Table 1 Rietveld refined fit parameters of positive electrode deposits from SLFBs potentiostatically charged at 1.8 V and 1.9 V

	Phase fraction		Reliability factors		α-PbO_2 lattice parameters ($P4_2/mnm$)			β-PbO_2 lattice parameters ($Pbcn$)		
Charge voltage	α	β	R_{wp}	R_b	*a*	*b*	*c*	*a*	*b*	*c*
1.8 V	41.(8)	59.(2)	9.78	6.70	4.97(8)	5.92(3)	5.44(0)	4.95(4)	4.95(5)	3.38(1)
1.9 V	96.(6)	3.(4)	12.70	8.75	4.99(3)	5.93(3)	5.44(8)	4.93(5)	4.93(4)	3.36(7)

described previously, in terms of the relationship between R_2 and overpotential. With slow charge-transfer kinetics and low overpotential, 1.46 V *vs.* Ag/AgCl, nucleation occurs slowly, favoring growth before the entire electrode surface is covered with PbO_2. At high overpotential, 1.64 V *vs.* Ag/AgCl, charge-transfer is two orders of magnitude higher; nucleation occurs very fast, as a multitude of small particles form and coalesce before growth becomes favorable.

Morphology and efficiency

Controlling the size of particles electrochemically deposited on a surface is commonly described in terms of their critical radius, which is inversely proportional to overpotential.[30] Fig. 7 shows the voltage profile of two batteries potentiostatically charged at 1.8 V and 2.0 V. They were both charged to a capacity of 1.37×10^{-1} A h and, therefore, had the same mass of PbO_2 deposited upon charge. As described previously, however, the different overpotentials resulted in large particle growth in the former and nanoparticle growth in the latter. Each battery was then galvanostatically discharged at 20 mA cm^{-2}. Fig. 7 shows that the battery initially charged at 2.0 V exhibited much better discharge capacity than the one charged at 1.8 V. While the Coulombic efficiency of the former was 95.1%, it was only 57.8% for the latter. This lost capacity resulted from the incomplete dissolution of PbO_2 into solvated Pb^{2+}. Indeed, the inset of Fig. 7 shows that a great deal more mass of PbO_2 was left behind on the positive electrode initially charged at 1.8 V. Of the mass deposited upon charge, 45.0% remained on the positive electrode charged at 1.8 V, compared to only 2.6% on the battery charged at 2.0 V. These results suggest that by tailoring reaction conditions to specifically form nanoparticle PbO_2, its dissolution at the positive electrode upon discharge is greatly enhanced. In forming larger PbO_2 particles, as is the case in conditions encouraging low overpotential or poor Pb^{2+} diffusion, reduction of PbO_2 into solvated Pb^{2+} is severely impeded.

One condition that is extremely influential to the morphology of PbO_2 deposited is flow rate. By submerging graphite electrodes in stirred cylindrical vessels, flow can be easily altered by adjusting the stir rate. Fig. 8 shows the 17th charge profile of three batteries subject to different stir rates. This figure demonstrates that with slow flow, the low charge voltage regime is extended. Under high flow rate conditions, however, the voltage profile primarily consists of its original plateau at ~2.0 V. The SEM images in Fig. 8 show the specific morphology of PbO_2 deposited at the end of each 17th charge. These images show that the slow flow associated with longer periods of low overpotential leads to larger particle formations. Since these large particles do not undergo PbO_2/Pb^{2+} dissolution as efficiently, this eventually leads to battery failure. One mechanism to prolong battery life and efficiency, therefore, is to increase and optimize flow. Indeed, Fig. 9 shows that batteries operating in this manner, stirred at 700 rpm, can achieve very

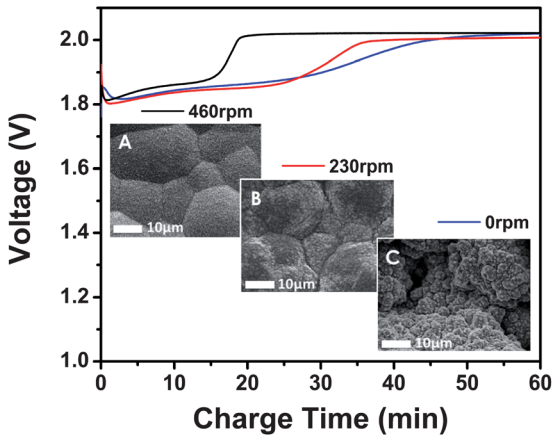

Fig. 8 Charge voltage, during the 17th cycle, of batteries having their electrolytes stirred at 460 rpm (black), 230 rpm (red), and 0 rpm (blue). The inset shows the deposit formed at the positive electrode of those batteries, A, B, and C, respectively.

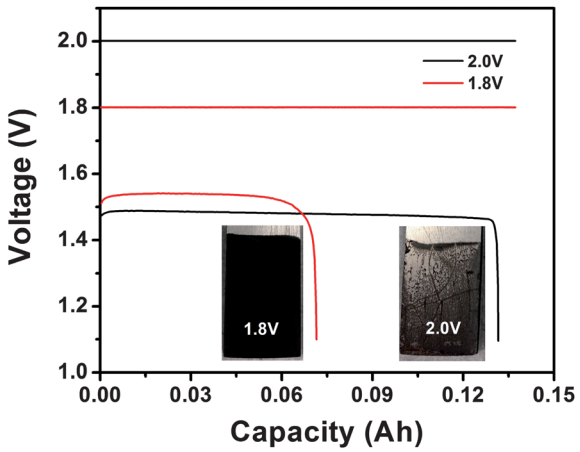

Fig. 7 Voltage of battery charged at 2.0 V (black) and 1.8 V (red) to a capacity of 1.37×10^{-1} A h and discharged to 1.1 V at 20 mA cm^{-2}. The inset shows an optical image of electrodes after full discharge – 45% and 2.6% of PbO_2 mass remaining on the left and right electrode, respectively.

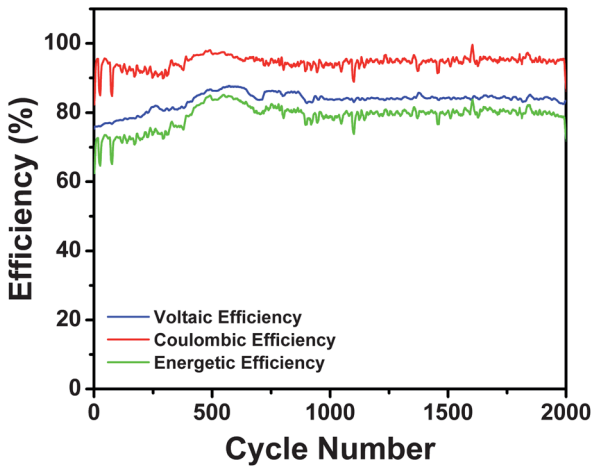

Fig. 9 Electrochemical efficiencies of SLFB charged at 20 mA cm^{-2} for 1 h and discharged at the same current density to 1.1 V, 2000 times at an average 79% energetic efficiency.

impressive performances. This figure shows a SLFB galvanostatically charged at 20 mA cm^{-2} for 1 h and discharged to 1.1 V, incorporating no additives, which cycled more than 2000 times at an average 79% energetic efficiency. The classic lead-acid battery has been known to achieve comparable numbers of cycles.[16] To our knowledge, however, this is the first time soluble lead flow batteries have successfully undergone so many cycles at such high efficiency. Recent reports describing "extended" cycle lives in SLFBs charged at 10 mA cm^{-2} typically range between 100 and 200 cycles at 65% efficiency.[13,14] Furthermore, additives such as hexadecyltrimethylammonium cation ($C_{16}H_{33}(CH_3)_3N^+$) or H_2O_2 have been commonly employed to reach even those modest numbers. Our work suggests that the reduction and dissolution of PbO_2 into solvated Pb^{2+} is the major hurdle to overcome in achieving long cycle lifetimes. In comparison, the dissolution of metallic Pb at the negative electrode is a much more kinetically favorable process.[6]

Conclusions

Several features associated with SLFB degradation have been reported here. The onset of electrochemical failure is marked by a simultaneous increase in voltaic efficiency and a decrease in Coulombic efficiency. Low Coulombic efficiency leads to both reduced cell capacity as well as build up of electrode deposits, which eventually leads to shorting. The increase in voltaic efficiency is due to the extension of a low charge voltage moiety following the first cycle, as well as a depression of the major charge voltage plateau. This has been attributed to the Pb^{2+}/PbO_2 redox reaction occurring at the positive electrode. Characterization of PbO_2 deposits formed under low and high voltage charging conditions were performed, therefore, to elucidate the mechanism of efficiency loss.

A slightly greater proportion of β-PbO_2 was determined to form under low voltage conditions, compared to α-PbO_2 (in a ratio of 59 : 41). When not taking into account the broadening of XRD peaks due to the formation of nanoparticles possessing small crystallite size and/or strain, α-PbO_2 appears to be formed in excess. At 2.0 V charging, however, when PbO_2 nanoparticles are uniformly distributed across the positive electrode, peak broadening in both α- and β-PbO_2 phases dominate, and each phase is clearly present. Large PbO_2 particles were consistently formed at low voltages, in contrast to the formation of nanoparticles at higher voltages. We attribute this to the faster and lower energy formation of small nuclei during conditions of high overpotential. High voltage charging was shown to increase charge-transfer kinetics and lead to instantaneous nucleation, as opposed to progressive nucleation and slow kinetics at lower charge voltages. The problem associated with depositing large particles is the difficulty in achieving efficient dissolution of PbO_2 back into solvated Pb^{2+} upon battery discharge. Nanoparticles are much better suited to accomplish this dissolution reaction. In order for SLFBs to emerge as a viable candidate for use in large-scale storage applications and compete with alternative technologies such as halogen–halide or vanadium redox batteries, they must be able to demonstrate extended cycle life capability. Here we demonstrate the conditions necessary to achieve this goal, as we have successfully cycled a SLFB more than 2000 times at 79% energetic efficiency. This breakthrough brings the low-cost SLFB back on the chart with other flow battery technologies for large-scale energy storage.

Acknowledgements

The authors are grateful for the financial support from the Department of Energy's Advanced Research Projects Agency (DOE-ARPAe), under contract #DE-AR0000124. This work is in collaboration with General Atomics and Affiliated Companies. Thanks go to our collaborators there, Matt Cassidy and Dr Leo Holland, who along with former collaborator, Dr David Keogh, initiated the project. We also appreciate the contributions from undergraduate research assistants at the University of California San Diego (UCSD), Han Nguyen and Michael Tang.

Notes and references

1 C. P. de Leon, A. Frias-Ferrer, J. Gonzalez-Garcia, D. A. Szanto and F. C. Walsh, *J. Power Sources*, 2006, **160**, 716–732.
2 P. Arora and Z. Zhang, *Chem. Rev.*, 2004, **104**, 4419–4462.
3 G. L. Soloveichik, in *Annual Review of Chemical and Biomolecular Engineering*, ed. J. M. Prausnitz, Annual Reviews, Palo Alto, 2011, vol. 2, pp. 503–527.
4 C. P. Zhang, S. M. Sharkh, X. Li, F. C. Walsh, C. N. Zhang and J. C. Jiang, *Energy Convers. Manage.*, 2011, **52**, 3391–3398.
5 M. D. Gernon, M. Wu, T. Buszta and P. Janney, *Green Chem.*, 1999, **1**, 127–140.
6 A. Hazza, D. Pletcher and R. Wills, *Phys. Chem. Chem. Phys.*, 2004, **6**, 1773–1778.
7 D. Pletcher and R. Wills, *Phys. Chem. Chem. Phys.*, 2004, **6**, 1779–1785.
8 A. Hazza, D. Pletcher and R. Wills, *J. Power Sources*, 2005, **149**, 103–111.
9 D. Pletcher and R. Wills, *J. Power Sources*, 2005, **149**, 96–102.
10 D. Pletcher, H. Zhou, G. Kear, C. T. J. Low, F. C. Walsh and R. G. A. Wills, *J. Power Sources*, 2008, **180**, 621–629.
11 D. Pletcher, H. Zhou, G. Kear, C. T. J. Low, F. C. Walsh and R. G. A. Wills, *J. Power Sources*, 2008, **180**, 630–634.
12 X. H. Li, D. Pletcher and F. C. Walsh, *Electrochim. Acta*, 2009, **54**, 4688–4695.
13 J. Collins, G. Kear, X. H. Li, C. T. J. Low, D. Pletcher, R. Tangirala, D. Stratton-Campbell, F. C. Walsh and C. P. Zhang, *J. Power Sources*, 2010, **195**, 1731–1738.
14 J. Collins, X. H. Li, D. Pletcher, R. Tangirala, D. Stratton-Campbell, F. C. Walsh and C. P. Zhang, *J. Power Sources*, 2010, **195**, 2975–2978.
15 R. G. A. Wills, J. Collins, D. Stratton-Campbell, C. T. J. Low, D. Pletcher and F. C. Walsh, *J. Appl. Electrochem.*, 2010, **40**, 955–965.
16 M. Skyllas-Kazacos, M. H. Chakrabarti, S. A. Hajimolana, F. S. Mjalli and M. Saleem, *J. Electrochem. Soc.*, 2011, **158**, R55–R79.

17 A. B. Velichenko, R. Amadelli, E. V. Gruzdeva, T. V. Luk'yanenko and F. I. Danilov, *J. Power Sources*, 2009, **191**, 103–110.
18 A. Oury, A. Kirchev and Y. Bultel, *Electrochim. Acta*, 2012, **63**, 28–36.
19 A. Oury, A. Kirchev, Y. Bultel and E. Chainet, *Electrochim. Acta*, 2012, **71**, 140–149.
20 P. Ruetschi, *J. Electrochem. Soc.*, 1992, **139**, 1347–1351.
21 A. A. Shah, X. Li, R. G. A. Wills and F. C. Walsh, *J. Electrochem. Soc.*, 2010, **157**, A589–A599.
22 I. Sires, C. T. J. Low, C. Ponce-de-Leon and F. C. Walsh, *Electrochim. Acta*, 2010, **55**, 2163–2172.
23 N. Munichandraiah, *J. Appl. Electrochem.*, 1992, **22**, 825–829.
24 A. C. Larson and R. B. Dreele, *General Structure Analysis System (GSAS)*, Los Alamos National Laboratory, 2000, pp. 86–748.
25 H. Y. Peng, H. Y. Chen, W. S. Li, S. J. Hu, H. Li, J. M. Nan and Z. H. Xu, *J. Power Sources*, 2007, **168**, 105–109.
26 A. Oury, A. Kirchev and Y. Bultel, *J. Electrochem. Soc.*, 2013, **160**, A148–A154.
27 H. Wang, D. W. Brandl, F. Le, P. Nordlander and N. J. Halas, *Nano Lett.*, 2006, **6**, 827–832.
28 A. J. Bard, R. Parsons and J. Jordan, *Standard Potentials in Aqueous Solutions*, Marcel Dekker, New York, 1985.
29 A. Milchev, W. S. Kruijt, M. Sluyters-Rehbach and J. H. Sluyters, *J. Electroanal. Chem.*, 1993, **362**, 21–31.
30 M. Paunovic and M. Schlesinger, *Fundamentals of Electrochemical Deposition*, Wiley-Interscience, New Jersey, 2nd edn, 2006.
31 H. Seiter, H. Fischer and L. Albert, *Electrochim. Acta*, 1960, **2**, 97–120.
32 B. M. Chen, Z. C. Guo, X. W. Yang and Y. D. Cao, *Trans. Nonferrous Met. Soc. China*, 2010, **20**, 97–103.
33 X. Li, D. Pletcher and F. C. Walsh, *Chem. Soc. Rev.*, 2011, **40**, 3879–3894.
34 C. Hamann and T. Ropke, *J. Solid State Electrochem.*, 2003, **7**, 525–528.